

Cite this article as: Li Changmin, Luo Hengjun, Zhao Ning, et al. Constitutive Model and Microstructure Evolution of As-extruded Ti-6554 Alloy Based on Temperature Rise Correction[J]. Rare Metal Materials and Engineering, 2025, 54(09): 2189-2198. DOI: <https://doi.org/10.12442/j.issn.1002-185X.20240451>.

ARTICLE

Constitutive Model and Microstructure Evolution of As-extruded Ti-6554 Alloy Based on Temperature Rise Correction

Li Changmin^{1,2}, Luo Hengjun², Zhao Ning³, Guo Shiqi², Wei Minggang², Xiang Wei¹, Cui Mingliang², Xie Jing¹, Huang Liang²

¹ China National Erzhong Group Deyang Wanhang Die Forging Co., Ltd, Deyang 618000, China; ² State Key Laboratory of Materials Processing and Die & Mould Technology, School of Materials Science and Engineering, Huazhong University of Science and Technology, Wuhan 430074, China; ³ Western Superconducting Technologies Co., Ltd, Xi'an 710018, China

Abstract: The hot deformation behavior of as-extruded Ti-6554 alloy was investigated through isothermal compression at 700–950 °C and 0.001–1 s⁻¹. The temperature rise under different deformation conditions was calculated, and the curve was corrected. The strain compensation constitutive model of as-extruded Ti-6554 alloy based on temperature rise correction was established. The microstructure evolution under different conditions was analyzed, and the dynamic recrystallization (DRX) mechanism was revealed. The results show that the flow stress decreases with the increase in strain rate and the decrease in deformation temperature. The deformation temperature rise gradually increases with the increase in strain rate and the decrease in deformation temperature. At 700 °C/1 s⁻¹, the temperature rise reaches 100 °C. The corrected curve value is higher than the measured value, and the strain compensation constitutive model has high prediction accuracy. The precipitation of the α phase occurs during deformation in the two-phase region, which promotes DRX process of the β phase. At low strain rate, the volume fraction of dynamic recrystallization increases with the increase in deformation temperature. DRX mechanism includes continuous DRX and discontinuous DRX.

Key words: as-extruded Ti-6554 alloy; temperature rise correction; constitutive model; microstructure evolution

1 Introduction

The excellent mechanical properties of Ti-6Cr-5Mo-5V-4Al alloy show good potential for application in critical load-bearing components in the aviation field^[1-2]. At present, the cogging of bar required for the load-bearing components can be conducted by hot extrusion to achieve the purpose of refining the as-cast microstructure. Because the plasticity of the material can be brought into full play under the action of three-dimensional compressive stress. After hot extrusion, it is necessary for the bar to forge to obtain parts with stable microstructure and mechanical properties^[3]. Meanwhile, the microstructure in as-extruded state shows significant differences compared with that in the as-cast state. Considering

that titanium alloy is a kind of difficult-to-deform material, and there are problems, such as large deformation-resistance and uneven microstructure in the forging process, it is necessary to systematically study the hot deformation behavior and microstructure evolution of as-extruded titanium alloys.

Thermal compression experiments have become an effective way to analyze the flow behavior and microstructure evolution of metal materials. Ding et al^[4] analyzed the hot deformation behavior of ZL270LF aluminum alloy, and found that the suitable processing parameters are 470–530 °C/0.01–1 s⁻¹. And continuous dynamic recrystallization (CDRX), discontinuous dynamic recrystallization (DDRX), and geometric dynamic recrystallization (GDRX) occurred during hot

Received date: October 24, 2024

Foundation item: National Key R&D Program of China (2022YFB3706901); National Natural Science Foundation of China (52274382); Key Research and Development Program of Hubei Province (2022BAA024)

Corresponding author: Huang Liang, Ph. D., Professor, State Key Laboratory of Materials Processing and Die & Mould Technology, School of Materials Science and Engineering, Huazhong University of Science and Technology, Wuhan 430074, P. R. China, E-mail: huangliang@hust.edu.cn

Copyright © 2025, Northwest Institute for Nonferrous Metal Research. Published by Science Press. All rights reserved.

deformation. Feng et al^[5] analyzed the hot deformation behavior of the dual-phase Mg-Li alloy, and found that the α -Mg phase was transformed into the β -Li phase, which precipitated in the α -Mg phase in the form of spheroidization. At the same time, DRX is easy to occur in the β -Li phase, but is retarded in the α -Mg phase. Wang et al^[6] studied DRX behavior of a new nickel-based superalloy, and found that both DDRX and CDRX coexist at low temperatures and low strain rates. With the increase in temperature, CDRX becomes weaker, while DDRX becomes stronger with the increase in strain. Cai et al^[7] studied the hot deformation behavior of equiatomic FeCrMnNi high-entropy alloy, and found that the deformation microstructure is closely related to the power dissipation efficiency. When the power dissipation efficiency is 28%, DRX volume fraction is 17.6%. When the power dissipation efficiency increases to 38%, DRX volume fraction increases to 37.5 %. Shi et al^[8] analyzed the high temperature deformation behavior and recrystallization mechanism of Ti-55511 alloy, and found that with the increase in deformation temperature, DRX mechanism gradually transforms from DDRX to CDRX.

In the process of hot deformation, the stress-strain curve is an important mean to reflect the flow stress of the material and to measure the processing performance of the material. The heat generated during the deformation process of the sample, especially at high strain rates, is difficult to dissipate effectively, resulting in a significant temperature rise inside the sample^[9]. This will cause the measured value of the flow stress to deviate from the true value. Therefore, in order to deeply analyze the high temperature deformation behavior of titanium alloy and accurately obtain the stress-strain curve during hot compression, it is necessary to consider the influence of temperature rise on the curve. At present, researchers have conducted temperature rise correction in AZ31 magnesium alloy^[10], Ti-55531 alloy^[11], 300M steel^[12], and other materials.

In previous studies, the hot extrusion process of Ti-6554 has been extensively analyzed^[13]. At the same time, the researchers have also delved into the hot deformation behavior of the as-forged Ti-6554 alloy^[14-16]. Considering that the microstructure in as-extruded state is significantly different from that in as-cast state and as-forged state, it is necessary to analyze the hot deformation behavior of as-extruded alloys. Therefore, in this study, the hot deformation behavior of as-extruded Ti-6554 alloy was analyzed, the deformation temperature rise under different conditions was calculated, the stress-strain curve was corrected, and the constitutive equation was established. In addition, the microstructure evolution and DRX mechanism under different conditions were also analyzed.

2 Experiment

The material used in the present study was an extruded Ti-6554 alloy bar with a diameter of 70 mm. During the extrusion process, the extrusion speed was 40 mm/s, the extrusion temperature was 1100 °C, and the extrusion

ratio was 10^[13]. The chemical composition is 6.2Cr-5.3Mo-5.5V-4.0Al-0.17O-0.09N-Ti (wt%) and its initial microstructure is shown in Fig. 1^[13]. The phase transition point for this alloy is 785±5 °C. The samples were cylinders of \varnothing 8 mm×12 mm fabricated by wire cutting. The hot compression test was conducted on a Gleeble3800 thermal simulator, the deformation temperatures were 700–950 °C, and strain rates were 0.001–1 s⁻¹. In order to reduce friction, tantalum sheets were placed between the sample and the mold. Before hot compression, the samples were heated to the deformation temperature at a rate of 10 °C/s and held for 5 min. After hot compression, the samples were immediately water-cooled to obtain the deformed structure. Subsequently, the sample was cut along the compression direction by a wire cutting machine. The samples were mechanically ground and polished, followed by etching at room temperature in a solution of 2 mL hydrofluoric acid, 10 mL nitric acid, and 88 mL water. Microstructure characterization was performed on an optical microscope. Samples for electron backscattered diffractor (EBSD) were mechanically ground and then electropolished in the mixed solution of 70 mL methanol, 20 mL ethylene glycol, and 10 mL perchloric acid. EBSD used an OXFORD-NordlysMax system with a step of 0.5–1.0 μ m.

3 Results and Discussion

3.1 Stress-strain curve

Fig. 2 shows the stress-strain curves under different conditions. Work hardening is dominant in the early deformation stage, and dislocation density increases rapidly. At the same time, with the increase in strain, the flow stress increases rapidly to the peak. Subsequently, various softening mechanisms appear, such as DRX and dynamic recovery (DRV). The flow stress shows an obvious downward trend. When the work hardening and dynamic softening reach equilibrium, the flow curve reaches a stable state. In addition, it can be found that the flow stress of the as-extruded Ti-6554 alloy is significantly affected by the deformation parameters, and gradually increases with the increase in strain rate and the decrease in deformation temperature. At 700 °C/0.001 s⁻¹, the curve drops very significantly, while in the single-phase region the drop is very small. This shows that the softening mechanism in the two-

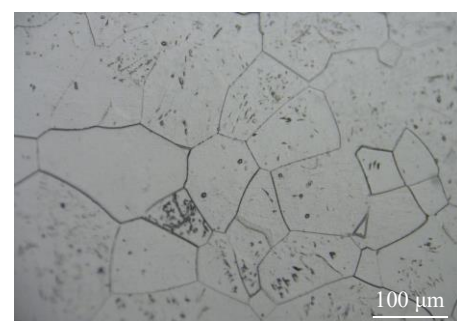


Fig.1 Initial microstructure of as-extruded Ti-6554 alloy

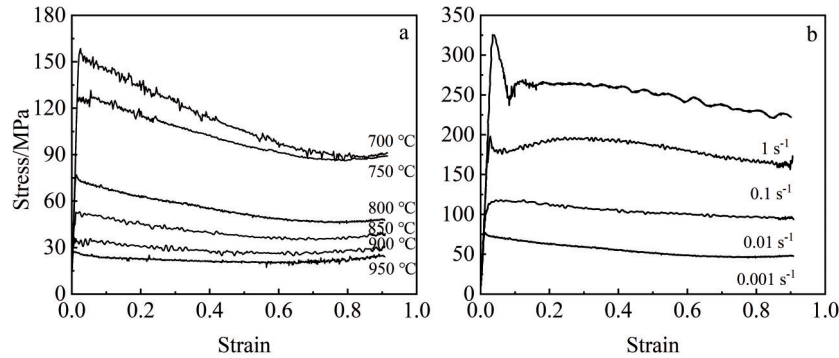


Fig.2 Stress-strain curves of as-extruded Ti-6554 alloy under different conditions: (a) 0.001 s^{-1} ; (b) $800\text{ }^{\circ}\text{C}$

phase region is different from that in the single-phase region.

3.2 Deformation heat effect

The deformation heat effect is a common phenomenon in the hot deformation process of titanium alloy. The deformation heat effect will cause the actual deformation temperature of titanium alloy to be higher than the heating temperature, which is beneficial to promote dislocation rearrangement and reduce dislocation density^[17]. The increase in deformation temperature can further promote DRX and DRV, and enhance the softening effect of titanium alloy. In addition, due to the poor thermal conductivity of titanium alloy, the deformation temperature rise will lead to the generation of local plastic flow^[18]. At present, under the same deformation temperature and deformation amount, the influence of deformation heat effect on the flow stress of titanium alloy mainly depends on the strain rate. The temperature rise in the deformation process is calculated by the following formula^[10,19]:

$$\Delta T = \frac{0.95\eta \int_0^{\varepsilon} \sigma d\varepsilon}{\rho c} \quad (1)$$

$$\eta = 0.316 \lg \dot{\varepsilon} + 0.95$$

where ΔT is deformation temperature rise, ε is strain, $\dot{\varepsilon}$ is strain rate, σ is stress, η is adiabatic correction factor, $\int_0^{\varepsilon} \sigma d\varepsilon$ is the area under the uncorrected stress and strain curve, ρ is materials density (4.5 g/cm^3), and c is specific heat capacity of $0.52\text{ J/(g}\cdot\text{K)}$. In this study, the deformation heat under different conditions is calculated, as shown in Fig. 3. The deformation temperature rise gradually increases with the increase in strain rate and the decrease in deformation temperature. At $700\text{ }^{\circ}\text{C}/1\text{ s}^{-1}$, the temperature rise reaches $100\text{ }^{\circ}\text{C}$. Xu et al^[20] found that the temperature rise of Ti-17 alloy at $780\text{ }^{\circ}\text{C}/10\text{ s}^{-1}$ is $80\text{ }^{\circ}\text{C}$, and the change trend of temperature rise is also consistent with this study. Therefore, at $700\text{ }^{\circ}\text{C}/1\text{ s}^{-1}$, the reason for the obvious softening of the stress-strain curve may be related to the deformation heat effect.

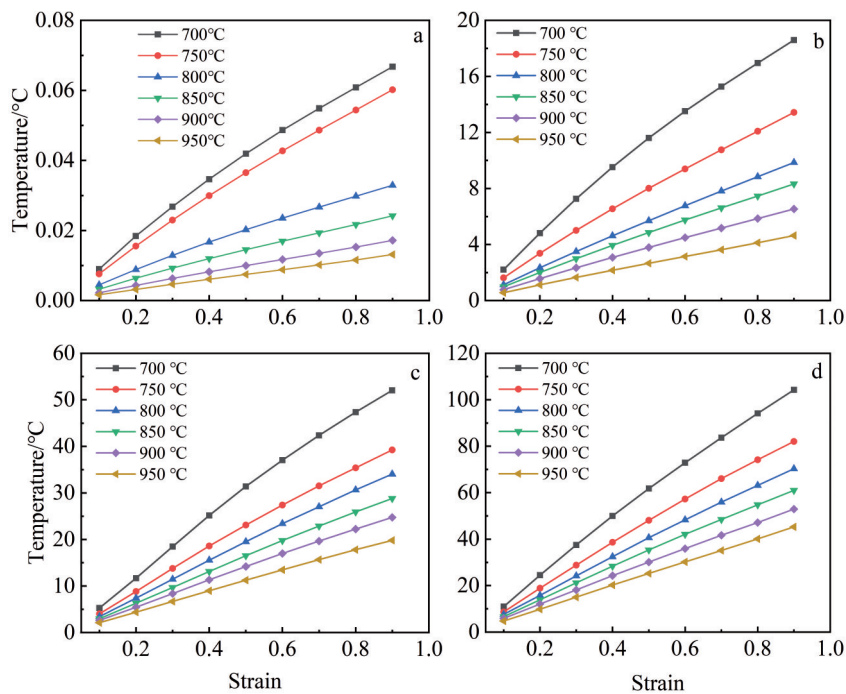


Fig.3 Temperature rise of as-extruded Ti-6554 alloy under different strain rates: (a) 0.001 s^{-1} ; (b) 0.01 s^{-1} ; (c) 0.1 s^{-1} ; (d) 1 s^{-1}

3.3 Stress-strain curve correction

At high strain rates, due to the short deformation time, the thermocouple can only measure the temperature of sample surface. And the Gleeble system is difficult to adjust the temperature change, which significantly reduces the deformation resistance. Therefore, it is necessary to correct the curve. At present, at a given strain and strain rate, the stress-strain curve should be corrected by the following formula^[11]:

$$\bar{\sigma} = \sigma - \frac{d\sigma}{dT} \Big|_{\dot{\varepsilon}, \varepsilon} \Delta T \quad (2)$$

where T is deformation temperature, σ is true stress (corrected), $\bar{\sigma}$ is the measured stress (uncorrected). Fig. 4 shows the comparison between the corrected curve and the uncorrected curve. It can be found that there is no significant difference between the measured value and the corrected value at a low strain rate. Therefore, the deformation heat effect at a low strain rate can be ignored. At high strain rates, the corrected value is significantly higher than the measured value, which means that temperature rise can effectively promote flow softening, as shown in Fig.4d.

3.4 Constitutive equation

The effect of strain on flow stress is not as significant as that of strain rate and deformation temperature. Therefore, the influence of strain on flow stress can be ignored, and it is proposed that the relationship between flow stress, strain rate and deformation temperature in steady-state flow stage conforms to three Arrhenius models, namely exponential function type, power function type, and hyperbolic sine type. Their expressions are as follows^[21]:

$$\dot{\varepsilon} \exp(Q/RT) = A_1 \sigma^{n_1} \quad (3)$$

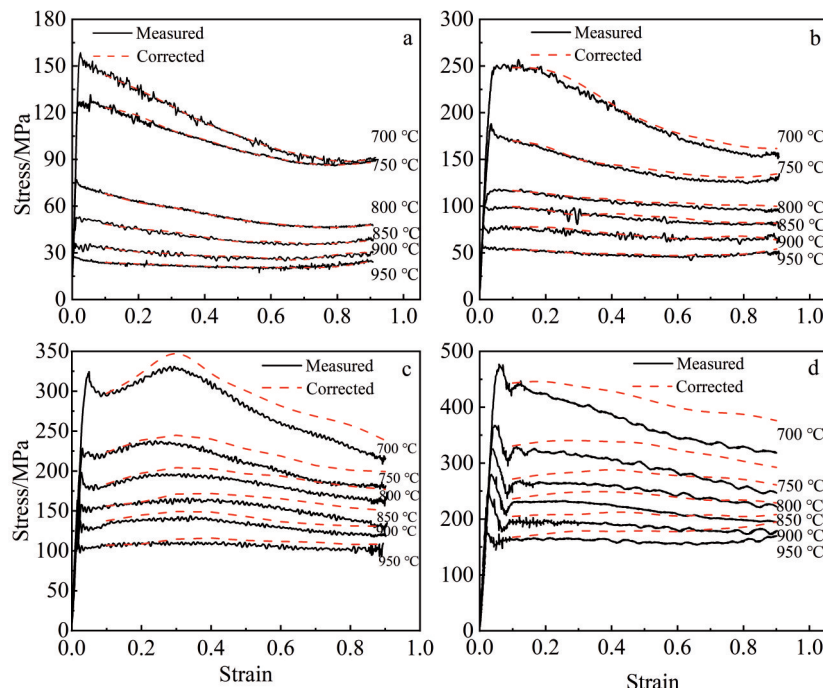


Fig.4 Comparison of stress-strain curves before and after correction under different strain rates: (a) 0.001 s^{-1} ; (b) 0.01 s^{-1} ; (c) 0.1 s^{-1} ; (d) 1 s^{-1}

$$\dot{\varepsilon} \exp(Q/RT) = A_2 \exp(\beta \sigma) \quad (4)$$

$$\dot{\varepsilon} \exp(Q/RT) = A \sinh(\alpha \sigma)^n \quad (5)$$

where $\dot{\varepsilon}$ represents the strain rate, Q represents the thermal deformation activation energy, R represents the gas constant, σ represents the flow stress, T represents the deformation temperature, n_1 and n represent material parameters related to the strain rate sensitivity index, and A , A_1 , A_2 , α , and β represent material constants. In order to calculate the parameters in the above equations, take the natural logarithm of Eq.(3-5):

$$\ln \dot{\varepsilon} = \ln A_1 + n_1 \ln \sigma - Q/RT \quad (6)$$

$$\ln \dot{\varepsilon} = \ln A_2 + \beta \sigma - Q/RT \quad (7)$$

$$\ln \dot{\varepsilon} = \ln A + n \ln [\sinh(\alpha \sigma)] - Q/RT \quad (8)$$

According to Eq.(6) and Eq.(7), it can be found that $\ln \dot{\varepsilon}$ has an obvious linear relationship with $\ln \sigma$ and σ , respectively. Subsequently, the peak stress in the stress-strain curve is selected for linear fitting, and the results are shown in Fig.5a-5b. n_1 and β are the average of reciprocal of the curve slope in the figure. The calculated values of n_1 and β are 4.8833 and 0.031, respectively. The value of α can be calculated by the following formula:

$$\alpha = \beta/n_1 \quad (9)$$

According to Eq.(9), the value of α under peak stress can be calculated to be 0.006347. In addition, according to Eq.(8), the thermal activation energy Q can be calculated by the following formula:

$$Q = R n k = R n \left[\frac{\partial \ln \sinh(\alpha \sigma_p)}{\partial (1/T)} \right]_{\dot{\varepsilon}} \quad (10)$$

where σ_p represents predicted flow stress, and n is the stress index, which is defined as:

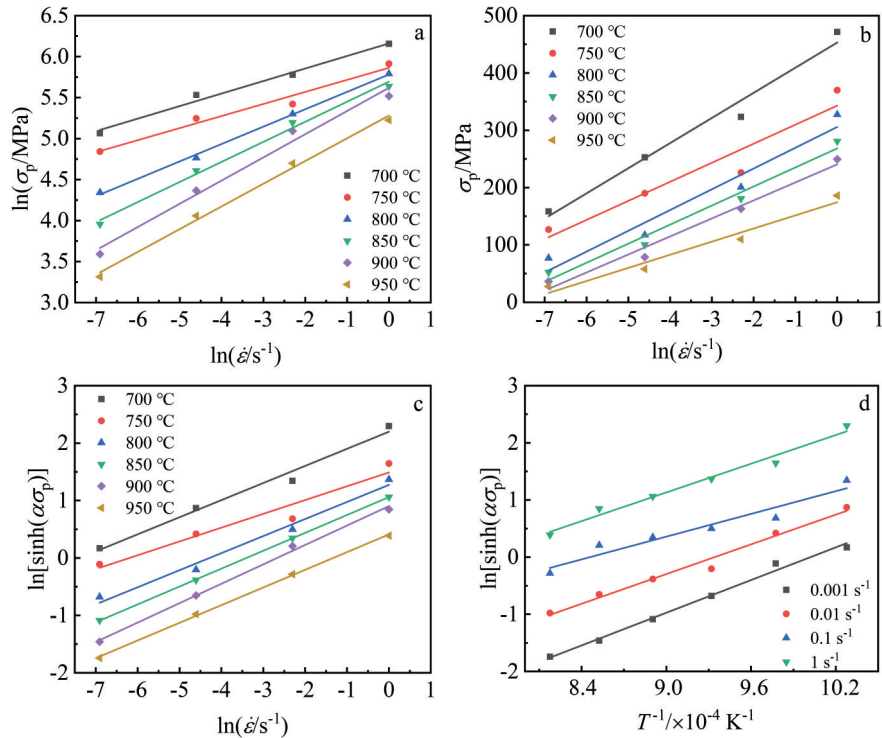


Fig.5 Relationships between $\ln\sigma$ and $\ln\dot{\varepsilon}$ (a), σ and $\ln\dot{\varepsilon}$ (b), $\ln[\sinh(\alpha\sigma_p)]$ and $\ln\dot{\varepsilon}$ (c), and $\ln[\sinh(\alpha\sigma_p)]$ and $1/T$ (d)

$$n = \left\{ \frac{\partial \ln\dot{\varepsilon}}{\partial \ln[\sinh(\alpha\sigma)]} \right\}_T \quad (11)$$

According to Eq. (10 – 11), the average values of the slopes of $\ln[\sinh(\alpha\sigma_p)] - \ln\dot{\varepsilon}$ and $\ln[\sinh(\alpha\sigma_p)] - 1/T$ can be determined (Fig. 5c – 5d), and then the values of Q and n are calculated to be 233.514 kJ/mol and 3.384, respectively. In addition, it was noted that the effect of deformation temperature and strain rate on the hot deformation behavior of the alloy can be expressed by the Zener-Hollomon parameter:

$$Z = \dot{\varepsilon} \exp(Q/RT) = A[\sinh(\alpha\sigma)]^n \quad (12)$$

Taking the natural logarithm of both sides of the Eq.(12):

$$\ln Z = \ln\dot{\varepsilon} + Q/RT = \ln A + n \ln[\sinh(\alpha\sigma)] \quad (13)$$

According to Eq.(13), it can be determined that there is a clear linear relationship between $\ln Z$ and $\ln[\sinh(\alpha\sigma)]$, and the fitting results are shown in Fig. 6. The intercept in the figure is the value of $\ln A$, which can be determined as 21.65. Therefore, the constitutive model of as-extruded Ti-6554 alloy under peak stress after temperature rise correction can be expressed as:

$$\dot{\varepsilon} = 2.533 \times 10^9 [\sinh(0.006347\sigma_p)]^{3.384} \exp(-233514/RT) \quad (14)$$

It can be seen from Fig. 4 that the strain significantly affects the flow stress. In fact, both the material constants and the thermal deformation activation energy are affected by the strain and follow a polynomial relationship^[22–24]. Obviously, as shown in Eq. (14), the Arrhenius constitutive model does not consider the effect of strain on the flow stress, which may lead to the low accuracy of the constitutive

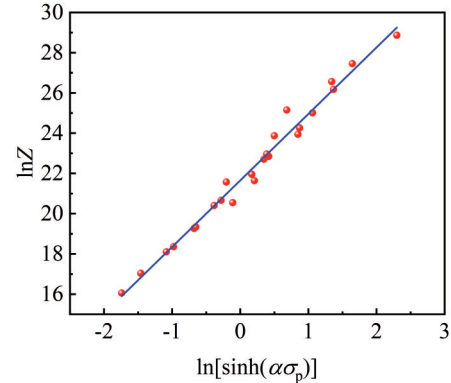


Fig.6 Relationship between $\ln Z$ and $\ln[\sinh(\alpha\sigma)]$

equation. Therefore, the Arrhenius constitutive model must be modified by strain compensation to improve its accuracy and achieve better predictability. The material constants and thermal deformation activation energy under different strains are shown in Fig. 7. It can be observed that the material constants and thermal activation energy change significantly with strain. According to Ref.[24], the relationship between true strain and material constants can be fitted by a fifth-order polynomial, as shown in Eq.(15), with the coefficients of the polynomial function presented in Table 1.

$$P = c_0 + c_1 \varepsilon + c_2 \varepsilon^2 + c_3 \varepsilon^3 + c_4 \varepsilon^4 + c_5 \varepsilon^5 + \dots \quad (15)$$

where P is material constant. After calculating the material constants and thermal activation energy under different strains, the strain-compensated Arrhenius constitutive model can be used to predict σ , as follows:

Table 1 Polynomial fitting results of α , n , Q , and $\ln A$ of Ti-6554 alloy in two-phase region

Coefficient	α/MPa^{-1}	n	$Q/\text{kJ}\cdot\text{mol}^{-1}$	$\ln A$
c_0	0.006 98	3.790 19	254.622 09	12.860 44
c_1	0.002 76	-2.864 84	131.398 80	-159.725 10
c_2	-0.014 22	-2.359 29	-1 495.117 67	341.672 47
c_3	0.045 43	19.039 22	3 143.961 35	-305.335 47
c_4	-0.052 49	-26.886 46	-2 772.778 96	100.152 24
c_5	0.019 41	12.657 48	897.130 47	12.860 44

$$\sigma = \frac{1}{\alpha_e} \ln \left\{ \left[\frac{\dot{\varepsilon} \exp(Q_e/RT)}{A_e} \right]^{\frac{1}{n_e}} + \left[\left(\frac{\dot{\varepsilon} \exp(Q_e/RT)}{A_e} \right)^{\frac{2}{n_e}} + 1 \right]^{\frac{1}{2}} \right\} \quad (16)$$

Fig. 8 is the comparison between the predicted flow stress and the experimental flow stress. It can be seen that the predicted values based on the constitutive model are basically consistent with the experimental values. Furthermore, the

prediction accuracy is quantitatively analyzed by correlation coefficient (R^2) and average absolute error (Δ), as follows^[23]:

$$R^2 = \frac{\sum_{i=1}^n (\sigma_E - \bar{\sigma}_E)(\sigma_p - \bar{\sigma}_p)}{\sqrt{\sum_{i=1}^n (\sigma_E - \bar{\sigma}_E)^2 (\sigma_p - \bar{\sigma}_p)^2}} \quad (17)$$

$$\Delta = \frac{1}{n} \sum_{i=1}^n \left| \frac{\sigma_E^i - \sigma_p^i}{\sigma_E^i} \right| \times 100\% \quad (18)$$

where σ_E represents experimental flow stress, σ_p represents predicted flow stress, n represents the total amount of data. The linear correlation coefficient between the predicted and experimental values is 0.988 (Fig.9), and the absolute value of average relative error is 5.75%. This shows that the hot deformation constitutive model of as-extruded Ti-6554 alloy considering strain compensation has high accuracy and can be used to predict the flow stress of the alloy in the hot deformation.

3.5 Microstructure analysis

Fig. 10 shows the microstructure of as-extruded Ti-6554 alloy under all deformation conditions. It can be found

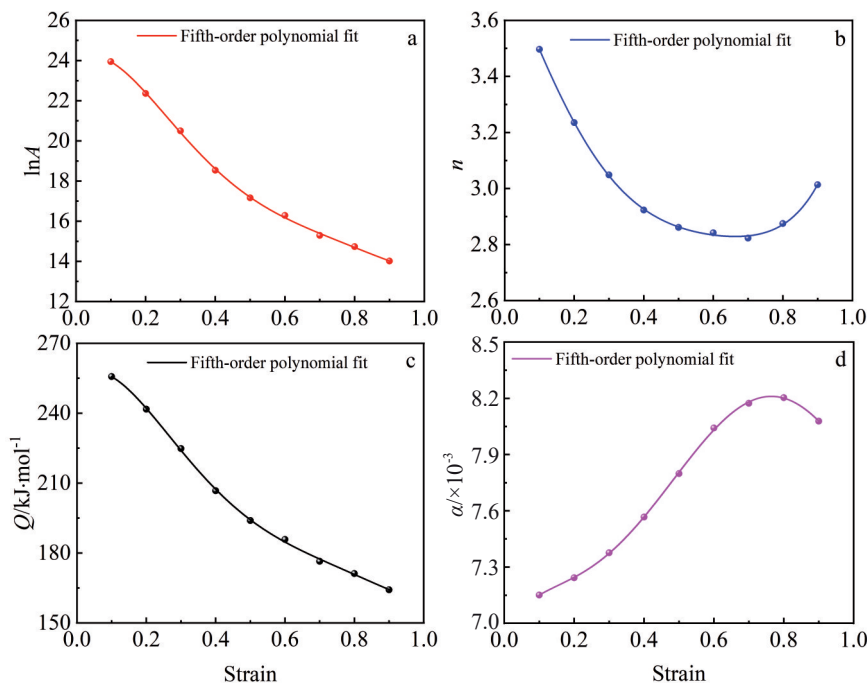


Fig.7 Variation of material constants and thermal activation energy with strain: (a) $\ln A$; (b) n ; (c) Q ; (d) α

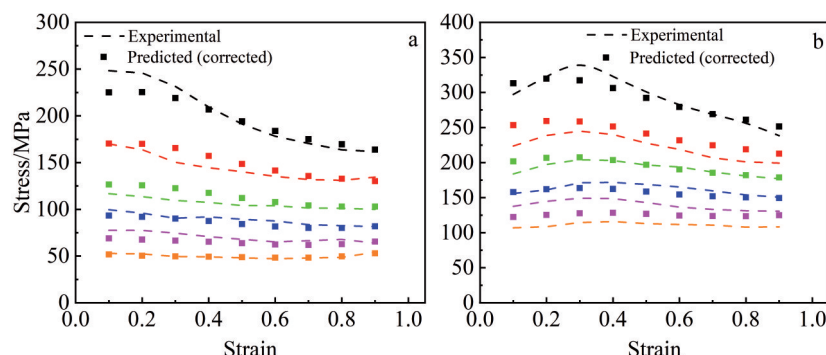


Fig.8 Comparison between experimental and predicted values of flow stress: (a) 0.01 s^{-1} ; (b) 0.1 s^{-1}

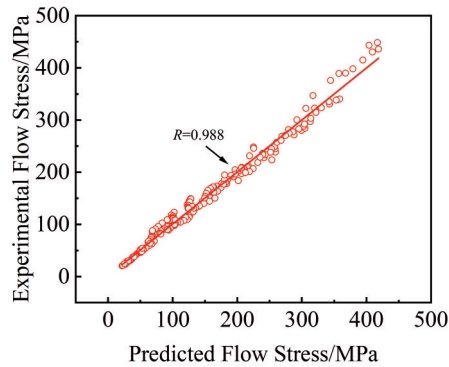


Fig.9 Correlation between experimental and predicted values

that some α phases precipitate at low strain rates in the two-phase region. With the increase in strain rate, the volume fraction of the α phase decreases significantly, and there is no

obvious change rule. This shows that the precipitation behavior of the α phase is not only affected by the strain rate, this phenomenon has also been reported in other studies^[25]. Notably, the original β grains become distinctly elongated at lower temperature and higher strain rates, indicating that DRV is the predominant deformation mechanism. Meanwhile, it should be noted that flow localization occurs at $700\text{ }^{\circ}\text{C}/1\text{ s}^{-1}$. This is related to the deformation temperature rise at low temperature and high strain rate, which further illustrates the necessity of temperature rise correction. In the single-phase region, obvious grain boundary bulging occurs at low strain rate, and many DRX grains are also observed. The increase in temperature provides sufficient driving force for DRX. At the same time, a low strain rate is beneficial to nucleation and growth of DRX grains. With the increase in deformation temperature, the volume fraction and grain size of

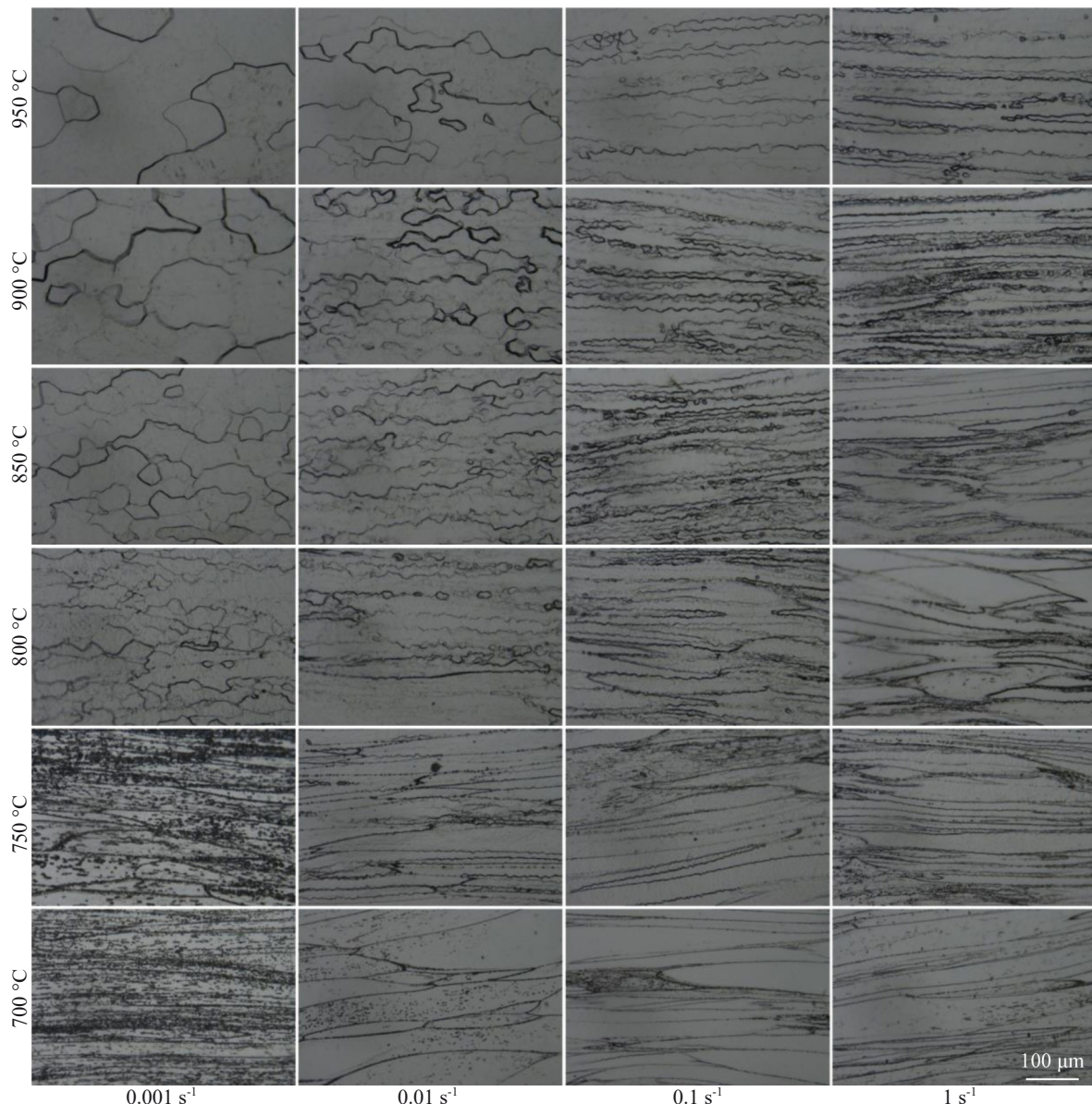


Fig.10 Microstructures of as-extruded Ti-6554 alloy under different conditions

DRX gradually increase. As the strain rate increases, the original β grains are also elongated. Different from low temperature, the grain boundary is serrated at 900 and 950 $^{\circ}\text{C}$.

EBSD is used to analyze the microstructure evolution in the deformation process of the two-phase region. Fig. 11 shows EBSD results at 700 $^{\circ}\text{C}$ with different strain rates. Black is high angle grain boundary (HAGB), blue is β phase, and red is α phase. The α phase precipitates at the grain boundary and interior of elongated β grain. It should be noted that some fine DRX grains are also found in Fig. 11a. Some studies have pointed out that during the deformation process, the incoherent phase interface can hinder the dislocation movement^[26-27], thus providing sufficient driving energy for the β -phase DRX process. Furthermore, the dislocation density will increase significantly at lower deformation temperature, which will further provide energy for DRX process. Therefore, the curve decreases significantly at low strain rate in the two-phase region (Fig. 2a).

3.6 DRX behavior

Fig.12 shows EBSD results at 900 $^{\circ}\text{C}/0.001 \text{ s}^{-1}$ and 900 $^{\circ}\text{C}/$

0.1 s^{-1} . Black is HAGB, and white is low angle grain boundary (LAGB). At 900 $^{\circ}\text{C}/0.001 \text{ s}^{-1}$, the lower strain rate is beneficial to the migration of grain boundaries, and most grain boundaries show obvious bulging, as shown in Fig. 12a, which is consistent with the results in Fig. 10. The grain boundary bulging can be regarded as the nucleation stage of DDRX. This is the phenomenon of strain-induced grain boundary migration, which belongs to DDRX process^[28-29]. The proportion of LAGBs in the sample is very low. At the same time, according to the cumulative misorientation inside the grains, it can be found that the cumulative orientation inside the grains does not exceed 15 $^{\circ}$ (Fig. 13a-13b). A similar phenomenon has been observed in previous studies^[30-32]. At 900 $^{\circ}\text{C}/0.1 \text{ s}^{-1}$, the grain boundaries gradually become straight, as shown in Fig. 12b. Higher strain rate promotes dislocation proliferation, but reduces the time of dynamic recrystallization nucleation and growth. According to the cumulative misorientation in Fig. 13c, it can be determined that CDRX occurs during the deformation process. In the existing research, 10 $^{\circ}$ - 15 $^{\circ}$ indicates the

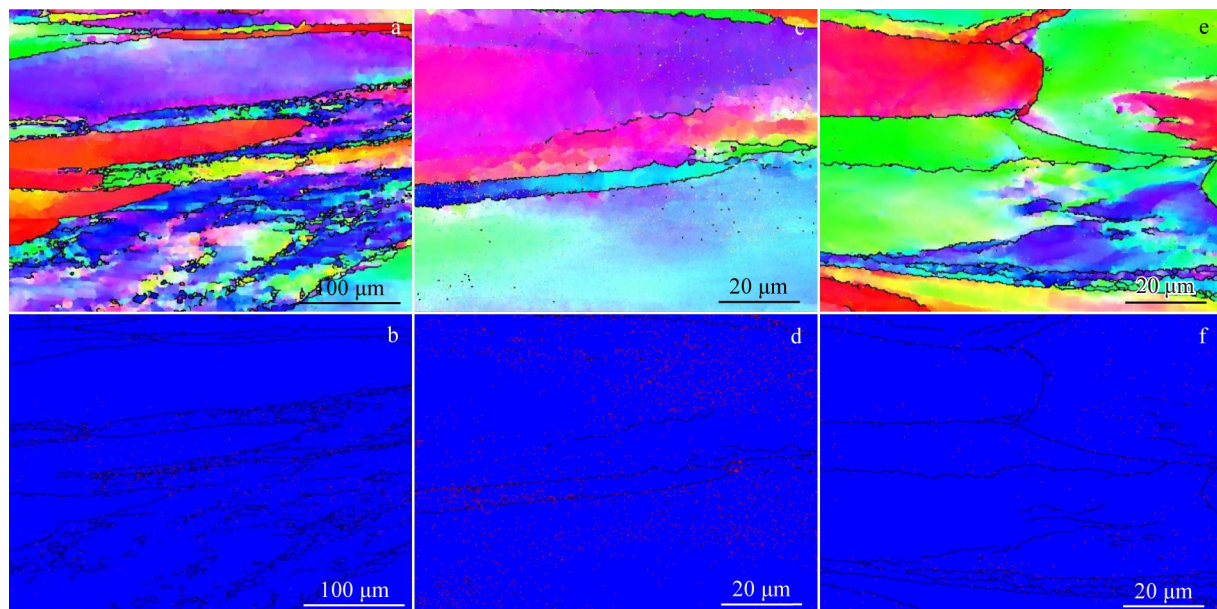


Fig.11 IPF maps (a, c, e) and phase distribution maps (b, d, f) of as-extruded Ti-6554 alloy at 700 $^{\circ}\text{C}$ with different strain rates: (a-b) 0.001 s^{-1} ; (c-d) 0.01 s^{-1} ; (e-f) 1 s^{-1}

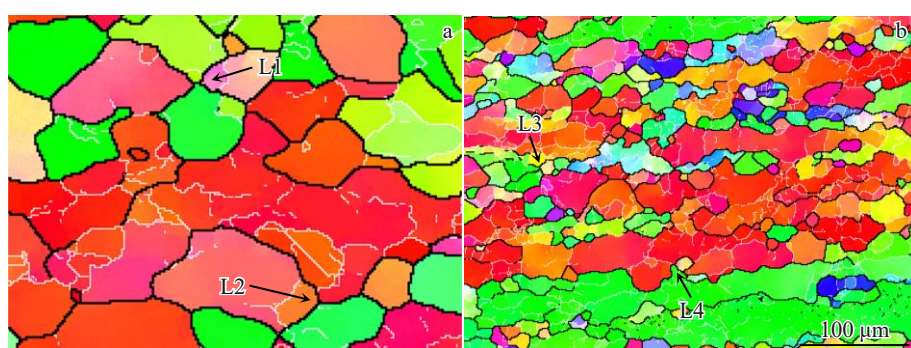


Fig.12 EBSD results of as-extruded Ti-6554 alloy at 900 $^{\circ}\text{C}$ with different strain rates: (a) 0.001 s^{-1} ; (b) 0.1 s^{-1}

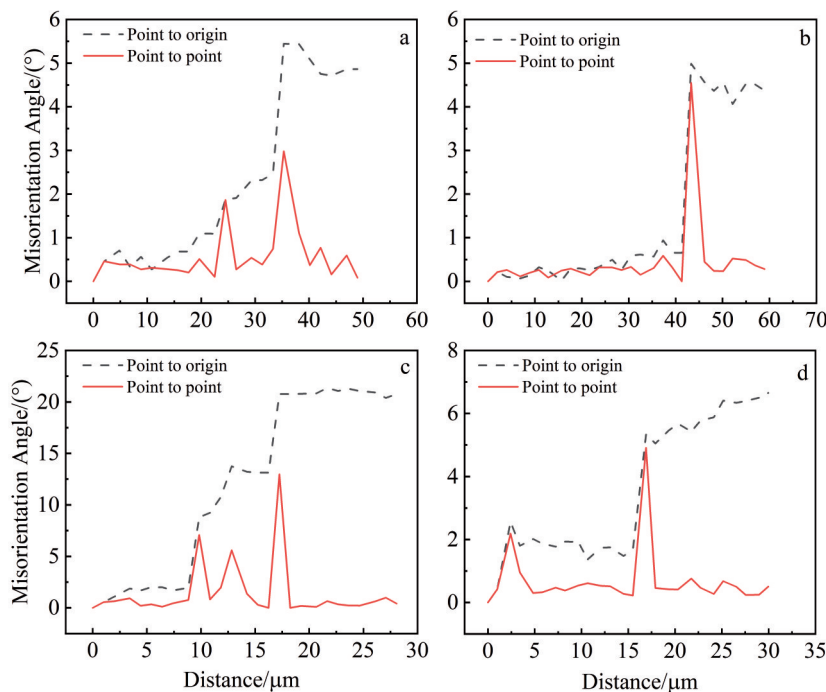


Fig.13 Misorientation angle along arrows marked in Fig.12: (a) L1; (b) L2; (c) L3; (d) L4

occurrence of CDRX^[33]. CDRX can be regarded as the recrystallization mechanism through progressive subgrain rotation. Meanwhile, DDRX also occurs under this condition (Fig.13d).

4 Conclusions

1) The flow stress increases with the increase in strain rate and the decrease in deformation temperature. The deformation temperature rise is more significant at a high strain rate. At 700 °C/1 s⁻¹, the temperature rise reaches 100 °C.

2) The corrected curve value is higher than the measured value. The constitutive model of as-extruded Ti-6554 alloy is established as follows:

$$\dot{\varepsilon} = 2.533 \times 10^9 \left[\sinh(0.006347 \sigma_p) \right]^{3.384} \exp(-233514/RT)$$

3) The precipitation of the α phase occurs during deformation in the two-phase region, which promotes DRX process of the β phase.

4) DRX mechanism includes CDRX and DDRX.

References

- 1 Li T, Kent D, Sha G et al. *Acta Materialia*[J], 2016, 106: 353
- 2 Wu C, Zhou Y J, Liu B. *Materials Science and Engineering A*[J], 2022, 838: 142745
- 3 Zhang S H, Xu Y, Shang Y L et al. *Journal of Materials Science & Technology*[J], 2001, 17(1): 113
- 4 Ding W W, Chen S H, Hu L W et al. *Rare Metal Materials and Engineering*[J], 2023, 52(12): 4086
- 5 Feng Y H, Sun C Y, Xu S N et al. *Rare Metal Materials and Engineering*[J], 2023, 52(4): 1227
- 6 Wang X M, Ding Y T, Bi Z N et al. *Rare Metal Materials and Engineering*[J], 2021, 50(12): 4201
- 7 Cai Z, Wu T D, Wei N et al. *Rare Metal Materials and Engineering*[J], 2022, 51(11): 4051
- 8 Shi S X, Ge J Y, Lin Y C et al. *Materials Science and Engineering A*[J], 2022, 847: 143335
- 9 Sun J Z, Li M Q, Li H. *Materials Science and Engineering A*[J], 2017, 697: 132
- 10 Ding X F, Zhao F Q, Shuang Y H et al. *Journal of Materials Processing Technology*[J], 2020, 276: 116325
- 11 Wu C, Huang L, Li C M. *Materials Science and Engineering A*[J], 2020, 773: 138851
- 12 Zhao M J, Huang L, Li C M et al. *Materials Science and Engineering A*[J], 2021, 810: 141031
- 13 Guo S Q, Huang L, Li C M et al. *The International Journal of Advanced Manufacturing Technology*[J], 2024, 131(7): 4233
- 14 Li C M, Huang L, Zhao M J et al. *Journal of Alloys and Compounds*[J], 2022, 924: 166481
- 15 Li C M, Huang L, Zhao M J et al. *Materials Science and Engineering A*[J], 2021, 814: 141231
- 16 Long S, Xia Y F, Wang P et al. *Journal of Alloys and Compounds*[J], 2019, 796: 65
- 17 Gao P F, Fu M W, Zhan M et al. *Journal of Materials Science & Technology*[J], 2020, 39: 56
- 18 Li C M, Huang L, Li C L et al. *Rare Metals*[J], 2022, 41(5): 1434
- 19 Jia Z, Yu L D, Wei B L et al. *Rare Metal Materials and Engineering*[J], 2022, 51(2): 461
- 20 Xu J W, Zeng W D, Zhou D D et al. *Journal of Alloys and Compounds*[J], 2018, 767: 285
- 21 Liu A J, Wang L, Cheng X W et al. *Rare Metal Materials and Engineering*[J], 2021, 50(12): 4201

- 22 Wen D X, Yue T Y, Xiong Y B et al. *Materials Science and Engineering A*[J], 2020, 803: 140491
- 23 Wang Y T, Li J B, Xin Y C et al. *Materials Science and Engineering A*[J], 2019, 768: 138483
- 24 Dong E T, Yu W, Cai Q W et al. *Materials Science and Engineering A*[J], 2019, 764: 138228
- 25 Matsumoto H, Kitamura M, Li Y P et al. *Materials Science and Engineering A*[J], 2014, 611: 337
- 26 Lin Y C, Huang J, He D G et al. *Journal of Alloys and Compounds*[J], 2019, 795: 471
- 27 Li C M, Huang L, Zhao M J et al. *Materials Science and Engineering A*[J], 2022, 850: 143571
- 28 Wang M J, Sun C Y, Fu M W et al. *Journal of Alloys and Compounds*[J], 2020, 820: 153325
- 29 Zhao Q Y, Yang F, Torrens R et al. *Materials Characterization*[J], 2019, 149: 226
- 30 Zhao J, Zhong J, Yan F et al. *Journal of Alloys and Compounds*[J], 2017, 710: 616
- 31 Zhong L W, Gao W L, Feng Z H et al. *Journal of Materials Science & Technology*[J], 2019, 35(10): 2409
- 32 Zang Q H, Yu H S, Lee Y S et al. *Materials Characterization*[J], 2019, 151: 404
- 33 Zang Q H, Yu H S, Lee Y S et al. *Journal of Alloys and Compounds*[J], 2018, 763: 25

基于温升修正的挤压态 Ti-6554 合金本构模型和微观组织演化

李昌民^{1,2}, 罗恒军², 赵 宁³, 郭士琦², 魏明刚², 向 伟¹, 崔明亮², 谢 静¹, 黄 亮²

(1. 中国第二重型机械集团德阳万航模锻有限责任公司, 四川 德阳 618000)

(2. 华中科技大学 材料科学与工程学院 材料成形与模具技术国家重点实验室, 湖北 武汉 430074)

(3. 西部超导材料科技股份有限公司, 陕西 西安 710018)

摘要: 在 700–950 °C、0.001–1 s⁻¹ 的等温压缩条件下, 研究了挤压态 Ti-6554 合金的热变形行为。计算了不同变形条件下的温升, 对曲线进行了温升修正, 建立了基于温升修正的挤压态 Ti-6554 合金的应变补偿本构模型。分析了不同条件下的微观组织演化规律, 揭示了动态再结晶 (DRX) 机制。结果表明, 流动应力随着应变速率的增加和变形温度的降低逐渐下降。变形温升随着应变速率的增加和变形温度的降低逐渐增加。在 700 °C/1 s⁻¹ 时, 温升达到 100 °C。修正后的曲线值高于测量值, 应变补偿本构模型预测精度较高。在两相区变形时析出了 α 相, 进而促进了 β 相的 DRX 过程。低应变速率下, 随着变形温度升高, 动态再结晶体积分数增加。DRX 机制包含连续 DRX 和非连续 DRX。

关键词: 挤压态 Ti-6554 合金; 温升修正; 本构模型; 微观组织演化

作者简介: 李昌民, 男, 1994 年生, 博士, 中国第二重型机械集团德阳万航模锻有限责任公司, 四川 德阳 618000, E-mail: lcm940214@126.com